Tuning Single-Molecule Magnetism in Dy^{3+} Complexes *via* Tris(aryl)alkoxide Ligand

Gautier Félix,*[a] Alexander N. Selikhov,[b,c] Max Kallio,[d] Veacheslav Vieru,[d] Anna V. Vologzhanina,[b] Elena V. Balagurova,[b] Yannick Guari,[a] Joulia Larionova*[a] and Alexander A. Trifonov*[b,c]

[a] ICGM, Univ. Montpellier, CNRS, ENSCM, Montpellier, France.

[b] A.N. Nesmeyanov Institute of Organoelement Compounds of Russian Academy of Sciences, 28 Vavilova str., bld. 1, 119334, Moscow, Russia.

[c] G.A. Razuvaev Institute of Organometallic Chemistry of Russian Academy of Sciences, 49 Tropinina str., GSP-445, 603950, Nizhny Novgorod, Russia.

[d] Maastricht Science Programme, Faculty of Science and Engineering, Maastricht University, Paul-Henri Spaaklaan 1 6229 EN, Maastricht, The Netherlands.

* Correspondence: G.F.: gautier.felix@umontpellier.fr; J.L.: joulia.larionova@umontpellier.fr; A.A.T. : trif@iomc.ras.ru.

Contents

Figures

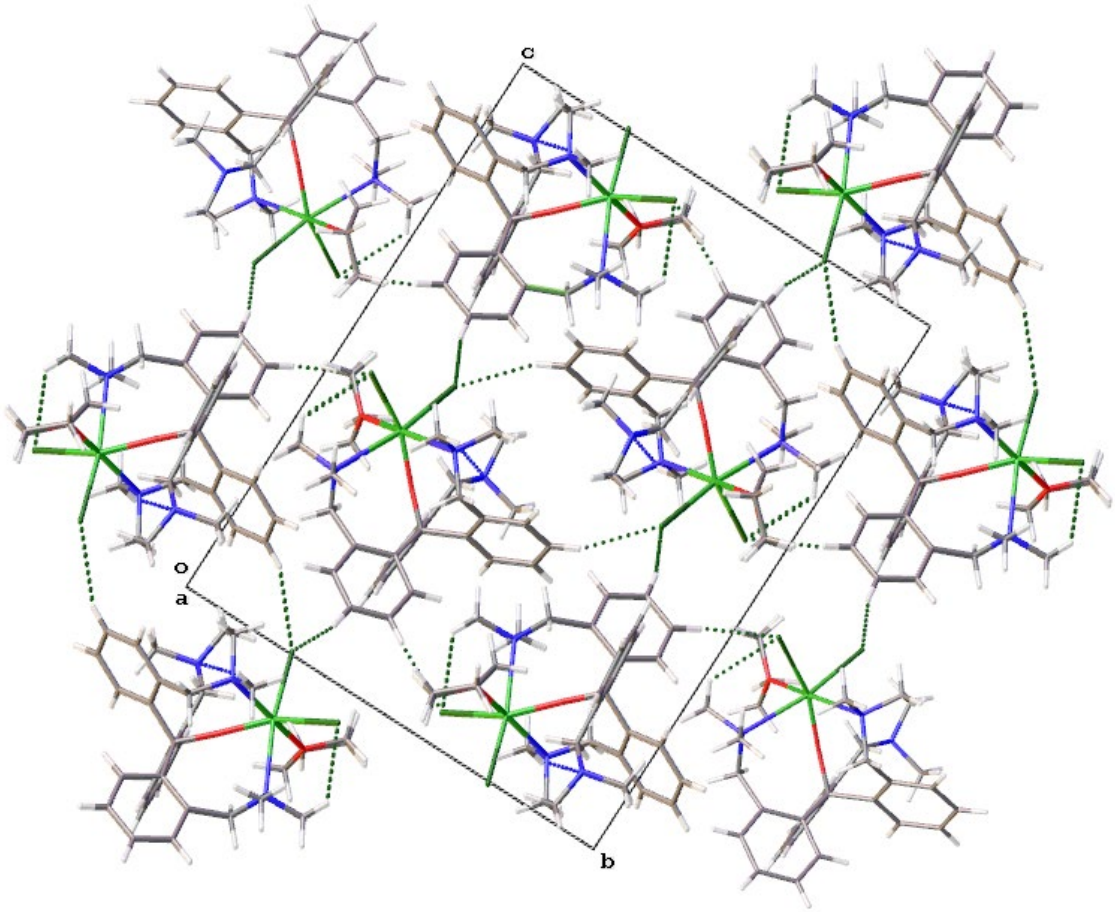

Figure S1. Crystal packing for **1** viewed along the crystallographic axis *a*. C–H…Cl and C–H…N interactions are dotted. Color code: C, grey; Cl, green; Dy, light-green; H – white; N – blue; O – red.

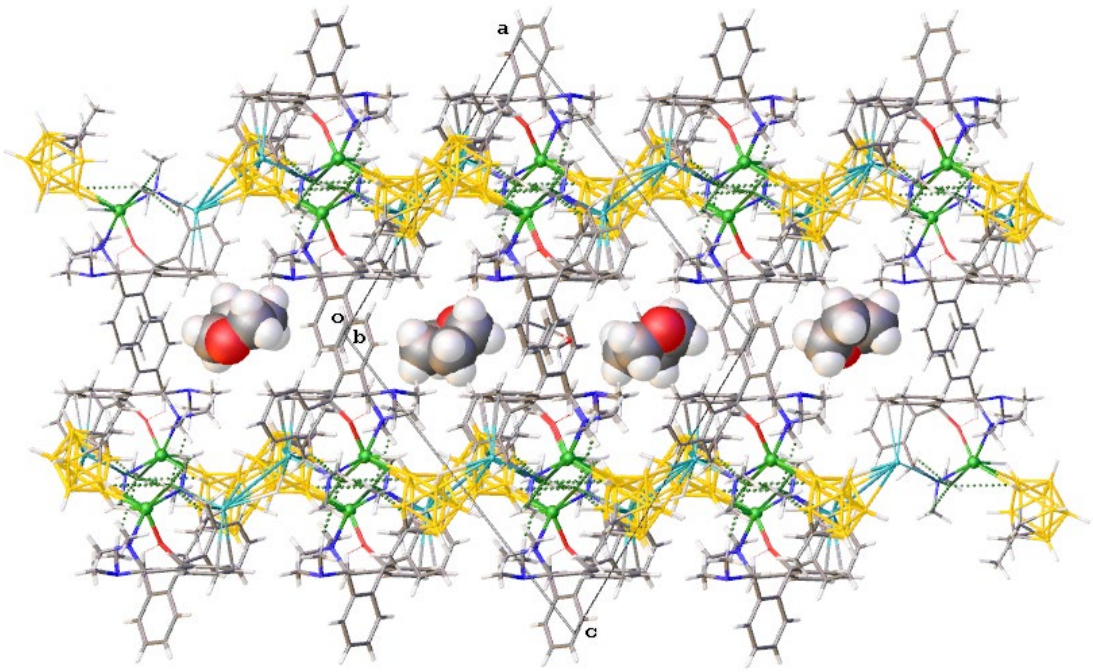

Figure S2. Crystal packing for *2* along the crystallographic axis *b*. THF molecules are depicted as van der Waals spheres. Inset: π…π stacking between aryl groups of neighboring layers. Color code: B, yellow; C, grey; Cl, green; Dy, light-green; H – white; K – light-blue; N – blue; O – red.

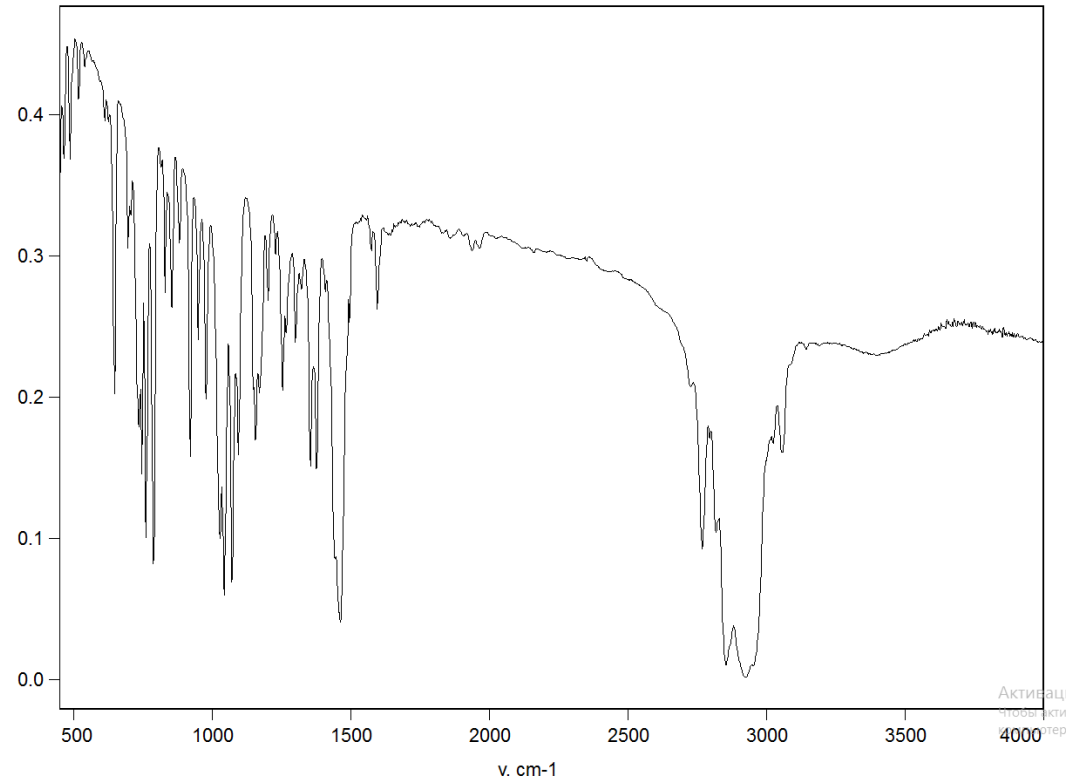

Figure S3. IR spectrum of complex **1** performed in Nujol.

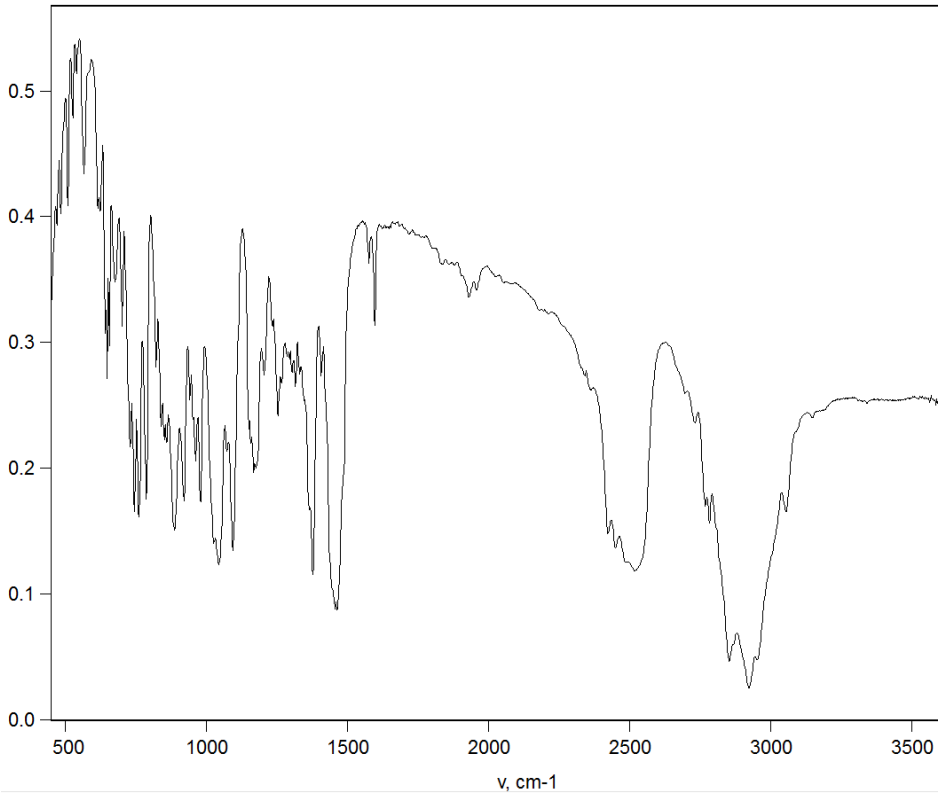

Figure S4. IR spectrum of complex **2** in Nujol.

Tables.

Table S1. Crystal data, data collection and structure refinement details for **1** and **2**.

	1	**2** · 0.5THF
Formula	$C_{32}H_{44}Cl_2DyN_3O_2$	$C_{34}H_{55}B_9ClDyKN_3O_{1.5}$
M	736.10	864.15
T, K	100	140
Crystal system	Monoclinic	Monoclinic
Space group	$P2_1/n$	$P2_1/n$
Z (Z')	4 (1)	4 (1)
a, Å	10.0997(2)	16.6956(6)
b, Å	15.8966(3)	16.1043(5)
c, Å	20.4614(4)	18.3134(6)
β, deg	94.589(1)	111.700(1)
V, Å^3	3274.56(11)	4575.0(3)
d_{calcd}, g·cm^{-3}	1.493	1.255
μ, mm^{-1}	24.77	18.12
F_{000}	1492	1756
$2\theta_{max}$, deg	56	65
Number of measured refl.	39447	57461
Number of independent refl. (R_{int})	7891	16590
Observed refl. [$I > 2\sigma(I)$]	6701	12369
Parameters	367	459
R_1 [$F^2 > 2\sigma(F^2)$]	0.0320	0.0368
wR_2 (all data)	0.0832	0.0936
$S(F^2)$	1.033	1.035
Residual density (d_{max}/d_{min}), e·Å^{-3}	1.416/-0.874	1.847/-1.469

Theoretical calculations.

1. Structures and Geometry Optimization using BP86-DFT.

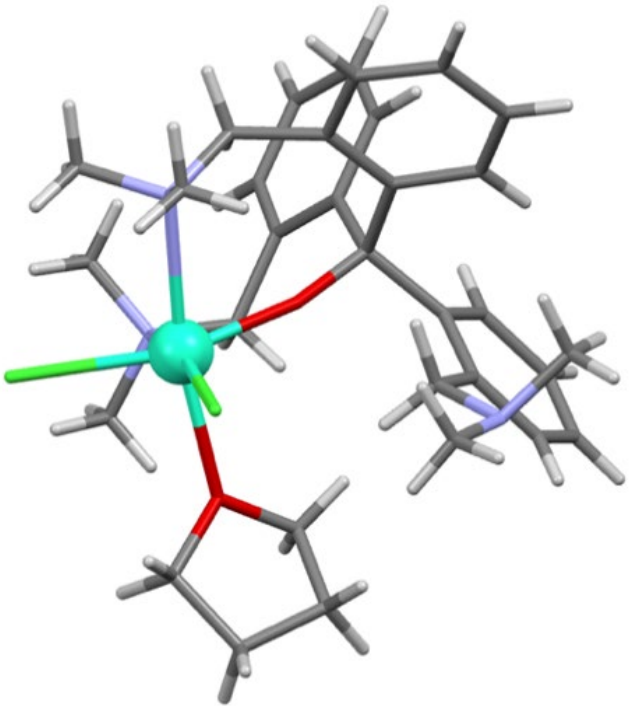

Figure S5. Structure of **1** used for CASSCF Calculations (Colour Code: Cyan=Dy, Red=O, Blue=N, Green=Cl, Grey=C, White=H).

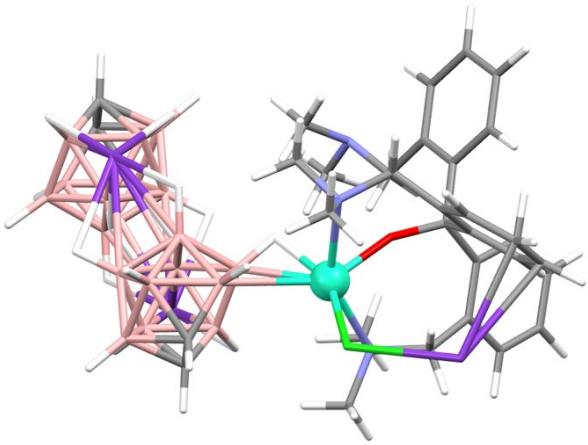

Figure S6. Top: Non-optimized structure **2** used for CASSCF calculations. Bottom: Structure **2*** used for CASSCF calculations after Geometry Optimization of the Hydrogen Atoms. (CC: Cyan=Dy, Red=O, Blue=N, Green=Cl, Grey=C, White=H, Pink=B, Purple=K).

The experimentally determined structure of **1** was used without further modification in the *ab initio* calculations. **2** crystallizes as a series of two-dimensional polymeric sheets, so we had to cut out an appropriately sized fragment for the *ab initio* calculations. Fortunately, the large distances between Dy-ions

(>8 Å within polymer sheets and >14 Å between sheets) in the crystalline structure of **2** allows for the treatment of this system by the regular CASSCF/CASPT2/RASSI-SO/SINGLE_ANISO-type calculations.[1–5] The choice of how to cut the structure for the *ab initio* calculations was motivated by keeping the carborane moieties intact and balancing the charges on the potassium ions. Finally, to speed up calculations, the methyl groups on the carboranes were replaced by hydrogen atoms in both **2** and **2***.

Because two hydrogens on the $[B_9H_9C_2Me_2]^{2-}$ are relatively close to the Dy-center, their positions may affect the energies of the crystal field levels. Therefore, the *ab initio* calculations were repeated for the structure with and without geometry optimization of the hydrogen atom positions to allow for comparison. The geometry optimization was carried out using the BP86 functional, with Zero-order regular approximation (ZORA) to account for relativistic effects on the lanthanide and Grimme's D3 dispersion correction for long-range interactions.[6–10] The ZORA-def2-SVP basis sets were used on all atoms except the lanthanide, which was treated with the SARC-ZORA-TZVP basis.[11,12] Resolution of identity was implemented with the SARC/J auxiliary basis set. Because DFT is not reliable in treating the open-shell, anisotropic Dy-center, it was replaced by Lu, which is chemically close to Dy but closed shell and isotropic. Convergence tolerances were set to 10^{-8} Hartree for SCF and 10^{-6} Hartree for geometry optimization with the TIGHTSCF and TIGHTOPT keywords in Orca 6.0. The optimized structure **2*** is referenced in the main text whenever **2** is discussed, and the non-optimized structure is only referenced in the supporting information.

2. *Ab Initio* Calculations.

The electronic structures and magnetic properties of **1** and **2** were calculated *ab initio*, using CASSCF/XMS-CASPT2/RASSI-SO/SINGLE_ANISO type calculations in OpenMolcas version 24.10.[1–5] The *ab initio* procedure was similar for **1** and **2**, and the non-optimized and geometry optimized **2** and **2*** were treated identically.

The one- and two-electron integrals, along with AMFI integrals were calculated using Seward with Cholesky decomposition threshold set to 10^{-7}. The Atomic Natural Orbitals with Relativistic Core Correlation (ANO-RCC) basis sets by Roos and Co-workers were used for all atoms due to their performance in CASSCF calculations.[13] Triple zeta quality was reserved for the lanthanide ion and all other atoms were treated at double zeta quality. The lanthanide and all atoms directly bound to it were treated with polarized basis sets. Detailed basis set information is shown in the tables below for **1** and **2**.

Table S2. Basis Sets used for the calculations of compound **1**.

ATOM	BASIS SET
DY	ANO-RCC-VTZP
CL	ANO-RCC-VDZP
O	ANO-RCC-VDZP
N (BOUND TO DY)	ANO-RCC-VDZP
N	ANO-RCC-VDZ
C	ANO-RCC-VDZ
H	ANO-RCC-VDZ

Table S3. Basis Sets used for the Calculations on 2 and 2*.

ATOM	BASIS SET
DY	ANO-RCC-VTZP
CL	ANO-RCC-VDZP
O	ANO-RCC-VDZP
N (BOUND TO DY)	ANO-RCC-VDZP
H (BOUND TO DY)	ANO-RCC-VDZP
B (BOUND TO DY)	ANO-RCC-VDZP
N	ANO-RCC-VDZ
H	ANO-RCC-VDZ
B	ANO-RCC-VDZ
C	ANO-RCC-VDZ
K	ANO-RCC-VDZ

All 21 sextet states, 224 quartet states, and 490 doublet states of Dy^{3+} (corresponding to CASSCF 9 electrons in 7 orbitals of 4f-type) were calculated using the RASSCF module in Molcas. The lowest lying 21 sextet states, 128 quartet states, and 130 doublet states were subsequently admixed using the RASSI program to calculate the spin-orbit coupling interaction.

To account for the electron correlation energy, extended Multi State Complete Active Space Perturbation Theory up to 2nd order (XMS-CASPT2) corrections were also calculated for low-lying CASSCF states.[5] Energy states higher than 25 000 cm^{-1} mix weakly with the ground state, so they were ignored to reduce complexity. Therefore, only the 18 lowest energy sextet states were calculated at the XMS-CASPT2 level (the ^{6}H and ^{6}F terms). The 18 resulting XMS-CASPT2 states were then admixed using RASSI to calculate the spin-orbit coupling correction to the CASPT2 energy spectrum. For the calculations on **2** and **2***, since the structures are much larger than **1**, the XMS-CASPT2 calculations were further simplified by freezing all inactive molecular orbitals with less than 0.05 of their density on the active site. The active site being the lanthanide and its first nearest neighbours, or the atoms with polarization functions in Table **S3**.

The magnetic properties of the compounds were then calculated using SINGLE_ANISO. This included the $\boldsymbol{g}$ tensors of the Kramers doublets in the ground level of Dy^{3+}, magnetic susceptibility against temperature from 0 to 300 K in 301 points, powder magnetization against applied field from 0 to 7 T in 71 points, and the matrix elements of the magnetic moment operator between low-lying states. The $\boldsymbol{g}$ tensors and energies of the states in the ground $^6H_{15/2}$ level of **1** are shown in **Table S4**. The energies of the states and the $\boldsymbol{g}$ tensors in the ground $^6H_{15/2}$ level of **2** and **2*** are shown in tables **S5** and **S6**.

Table S4. *g* Tensors, Energies of the Kramers Doublets in the Ground $^6H_{15/2}$ Level of **1** at CASSCF/RASSI-SO and XMS-CASPT2/RASSI-SO Levels of Accuracy.

Kramers Doublet	Energy / cm^{-1} **(CASSCF-SO)**	***g*** Tensor **(CASSCF-SO)**	Energy / cm^{-1} **(CASPT2-SO)**	***g*** Tensor **(CASPT2-SO)**
1	0	$g_X = 5.48*10^{-3}$ $g_Y = 8.57*10^{-3}$ $g_Z = 19.78$	0	$g_X = 7.86*10^{-3}$ $g_Y = 1.21*10^{-2}$ $g_Z = 19.86$
2	342.2188	$g_X = 2.16*10^{-1}$ $g_Y = 3.36*10^{-1}$ $g_Z = 16.50$	469.0843	$g_X = 3.38*10^{-1}$ $g_Y = 5.57*10^{-1}$ $g_Z = 16.20$
3	524.6478	$g_X = 1.80$ $g_Y = 2.51$ $g_Z = 12.93$	699.1636	$g_X = 2.06$ $g_Y = 2.79$ $g_Z = 12.78$
4	622.7726	$g_X = 8.01$ $g_Y = 7.93$ $g_Z = 3.04$	831.8069	$g_X = 9.34$ $g_Y = 7.04$ $g_Z = 3.28$
5	703.2579	$g_X = 1.40$ $g_Y = 3.51$ $g_Z = 8.08$	945.5555	$g_X = 1.01$ $g_Y = 4.02$ $g_Z = 9.63$
6	722.7296	$g_X = 1.03*10^{-1}$ $g_Y = 2.04$ $g_Z = 10.21$	974.8464	$g_X = 3.94*10^{-1}$ $g_Y = 4.47$ $g_Z = 12.13$
7	771.3616	$g_X = 5.51*10^{-1}$ $g_Y = 1.03$ $g_Z = 15.71$	1024.3389	$g_X = 6.91*10^{-1}$ $g_Y = 1.30$ $g_Z = 15.13$
8	932.3346	$g_X = 5.69*10^{-3}$ $g_Y = 1.03*10^{-2}$ $g_Z = 19.56$	1236.2812	$g_X = 1.63*10^{-2}$ $g_Y = 3.20*10^{-2}$ $g_Z = 19.54$

Table S5. Spin-orbit Coupled Eigenstate Energies of the Ground $^6H_{15/2}$ Level of **2** and **2*** at CASSCF/RASSI-SO and XMS-CASPT2/RASSI-SO Levels of Accuracy.

State	Energy / cm^{-1} (CASSCF-SO) **(2)**	Energy / cm^{-1} (CASSCF-SO) **(2*)**	Energy / cm^{-1} (CASPT2-SO) **(2)**	Energy / cm^{-1} (CASPT2-SO) **(2*)**
1	0	0	0	0
2	0	0	0	0
3	288.0276	276.2070	399.1737	385.4662
4	288.0276	276.2070	399.1737	385.4662
5	442.4206	420.9716	569.2253	547.3226
6	442.4206	420.9716	569.2253	547.3226
7	516.2843	497.9515	671.7753	650.4509
8	516.2843	497.9515	671.7753	650.4509
9	618.1669	595.8738	800.1496	773.9629
10	618.1669	595.8738	800.1496	773.9629
11	720.6259	684.2512	923.1767	875.2572
12	720.6259	684.2512	923.1767	875.2572
13	783.5158	734.3455	1002.0279	945.2807
14	783.5158	734.3455	1002.0279	945.2807
15	885.7163	822.1935	1145.7203	1070.0653
16	885.7163	822.1935	1145.7203	1070.0653

Table S6. *g* Tensors of the Kramers Doublets in the Ground $^6H_{15/2}$ Level of **2** and **2*** at CASSCF/RASSI-SO and XMS-CASPT2/RASSI-SO Levels of Accuracy.

Kramers Doublet	***g*** Tensor (CASSCF-SO) (**2**)	***g*** Tensor (CASSCF-SO) (**2***)	***g*** Tensor (CASPT2-SO) (**2**)	***g*** Tensor (CASPT2-SO) (**2***)
1	$g_X = 1.40*10^{-4}$ $g_Y = 5.05*10^{-4}$ $g_Z = 19.86$	$g_X = 1.46*10^{-3}$ $g_Y = 1.90*10^{-3}$ $g_Z = 19.85$	$g_X = 4.82*10^{-4}$ $g_Y = 1.14*10^{-3}$ $g_Z = 19.94$	$g_X = 2.01*10^{-3}$ $g_Y = 2.66*10^{-3}$ $g_Z = 19.94$
2	$g_X = 1.06*10^{-1}$ $g_Y = 1.73*10^{-1}$ $g_Z = 16.88$	$g_X = 1.47*10^{-1}$ $g_Y = 2.48*10^{-1}$ $g_Z = 16.84$	$g_X = 2.04*10^{-1}$ $g_Y = 3.51*10^{-1}$ $g_Z = 16.74$	$g_X = 2.61*10^{-1}$ $g_Y = 4.68*10^{-1}$ $g_Z = 16.67$
3	$g_X = 2.17$ $g_Y = 3.75$ $g_Z = 13.94$	$g_X = 2.34$ $g_Y = 3.77$ $g_Z = 13.73$	$g_X = 2.40$ $g_Y = 3.19$ $g_Z = 15.22$	$g_X = 2.77$ $g_Y = 3.64$ $g_Z = 14.43$
4	$g_X = 7.48$ $g_Y = 6.09$ $g_Z = 2.13$	$g_X = 7.28$ $g_Y = 6.44$ $g_Z = 2.23$	$g_X = 7.00$ $g_Y = 6.66$ $g_Z = 3.18$	$g_X = 7.30$ $g_Y = 6.22$ $g_Z = 2.85$
5	$g_X = 2.37$ $g_Y = 3.91$ $g_Z = 10.74$	$g_X = 2.15$ $g_Y = 3.76$ $g_Z = 10.90$	$g_X = 1.32$ $g_Y = 3.43$ $g_Z = 11.51$	$g_X = 1.01$ $g_Y = 3.11$ $g_Z = 11.96$
6	$g_X = 4.22*10^{-1}$ $g_Y = 1.10*10^{-1}$ $g_Z = 14.17$	$g_X = 3.51*10^{-1}$ $g_Y = 1.29$ $g_Z = 14.50$	$g_X = 6.22*10^{-1}$ $g_Y = 1.44$ $g_Z = 14.85$	$g_X = 5.00*10^{-1}$ $g_Y = 1.51$ $g_Z = 15.42$
7	$g_X = 3.53*10^{-1}$ $g_Y = 5.63*10^{-1}$ $g_Z = 18.10$	$g_X = 4.32*10^{-1}$ $g_Y = 7.13*10^{-1}$ $g_Z = 17.91$	$g_X = 4.26*10^{-1}$ $g_Y = 7.19*10^{-1}$ $g_Z = 17.91$	$g_X = 4.72*10^{-1}$ $g_Y = 8.13*10^{-1}$ $g_Z = 17.65$
8	$g_X = 3.05*10^{-2}$ $g_Y = 5.68*10^{-2}$ $g_Z = 19.62$	$g_X = 4.82*10^{-2}$ $g_Y = 1.00*10^{-1}$ $g_Z = 19.49$	$g_X = 3.34*10^{-2}$ $g_Y = 8.76*10^{-2}$ $g_Z = 19.52$	$g_X = 4.65*10^{-2}$ $g_Y = 1.20*10^{-1}$ $g_Z = 19.42$

The magnetic susceptibility and molar magnetization of **1** and **2*** calculated at XMS-CASPT2 level of theory are shown in the main text as **Figure 7**. Comparison of the CASSCF and XMS-CASPT2 susceptibility for **1** is shown below in **Figure S7**. The same comparison between **2** and **2*** at CASSCF and XMS-CASPT2 levels is shown in **Figure S8**.

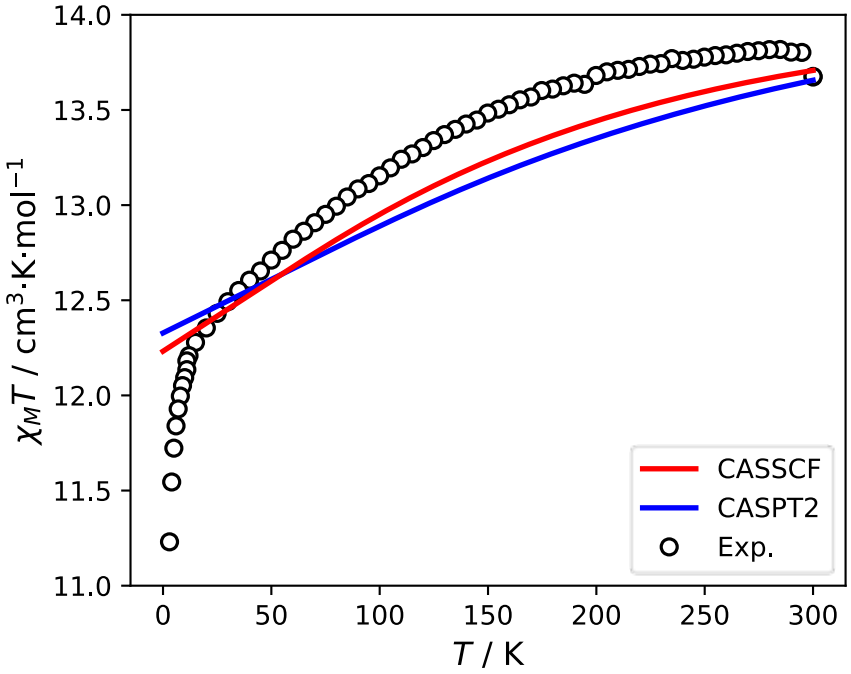

Figure S7. Comparison of *Ab Initio* Magnetic Susceptibility at CASSCF/RASSI-SO and XMS-CASPT2/RASSI-SO Levels of Theory for **1**.

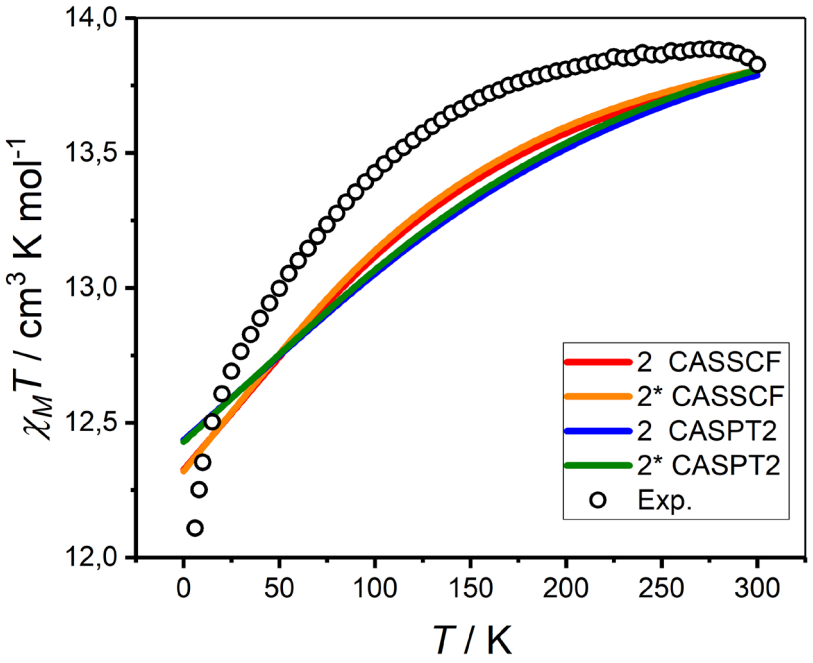

Figure S8. Comparison of *Ab Initio* Magnetic Susceptibility at CASSCF/RASSI-SO and XMS-CASPT2/RASSI-SO Levels of Theory for **2** and **2***.

The experimental magnetic susceptibility of **2** drops quickly at low temperature (Figure y, main text), which can be ascribed to weak anti-ferromagnetic interactions between adjacent Dy-ions. This can be modelled in a simple way by including a small coupling parameter which simulates this interaction. Fitting this parameter to the experimental data yielded a final value for the parameter of $J_Z = -0.02$. The magnetic susceptibility curve of **2*** with this coupling parameter is shown in the main text.

The main quantization axis of the ground doublet is shown for both **1** and **2*** in the figures below. The crystal field parameters *B(k, q)* of rank 2, 4, and 6 are shown in **Table S7** for all the calculated compounds at XMS-CASPT2/RASSI-SO level of theory.

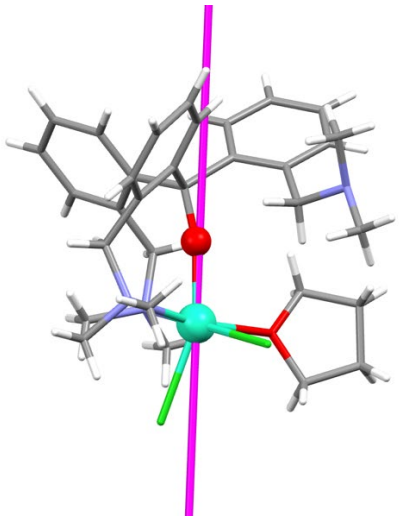

Figure S9. Main Quantization Axis (Magenta) of the Ground Doublet of **1.**

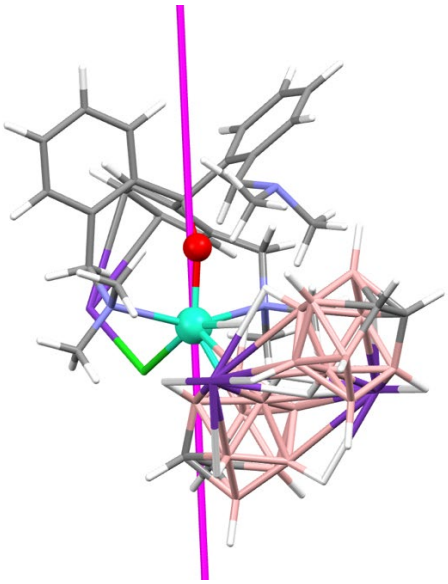

Figure S10. Main Quantization Axis (Magenta) of the Ground Doublet of 2*.

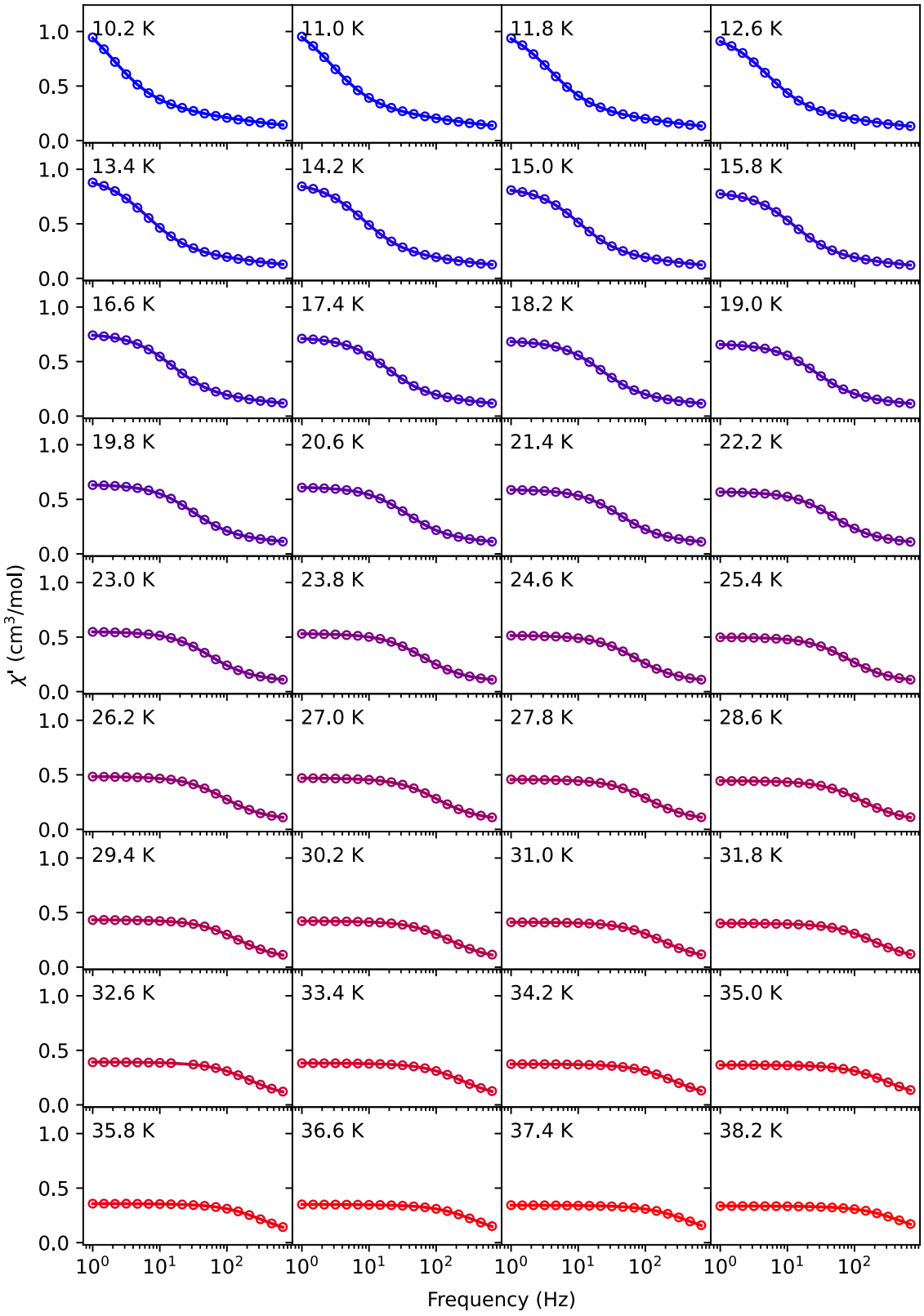

Figure S11. Frequency dependence of χ' for compound **1** measured at different temperatures ranging from 10.2 to 38.2 K under zero applied magnetic field. Solid circles represent experimental data, and lines correspond to theoretical fits using the Cole–Cole equation for multiple relaxation processes.

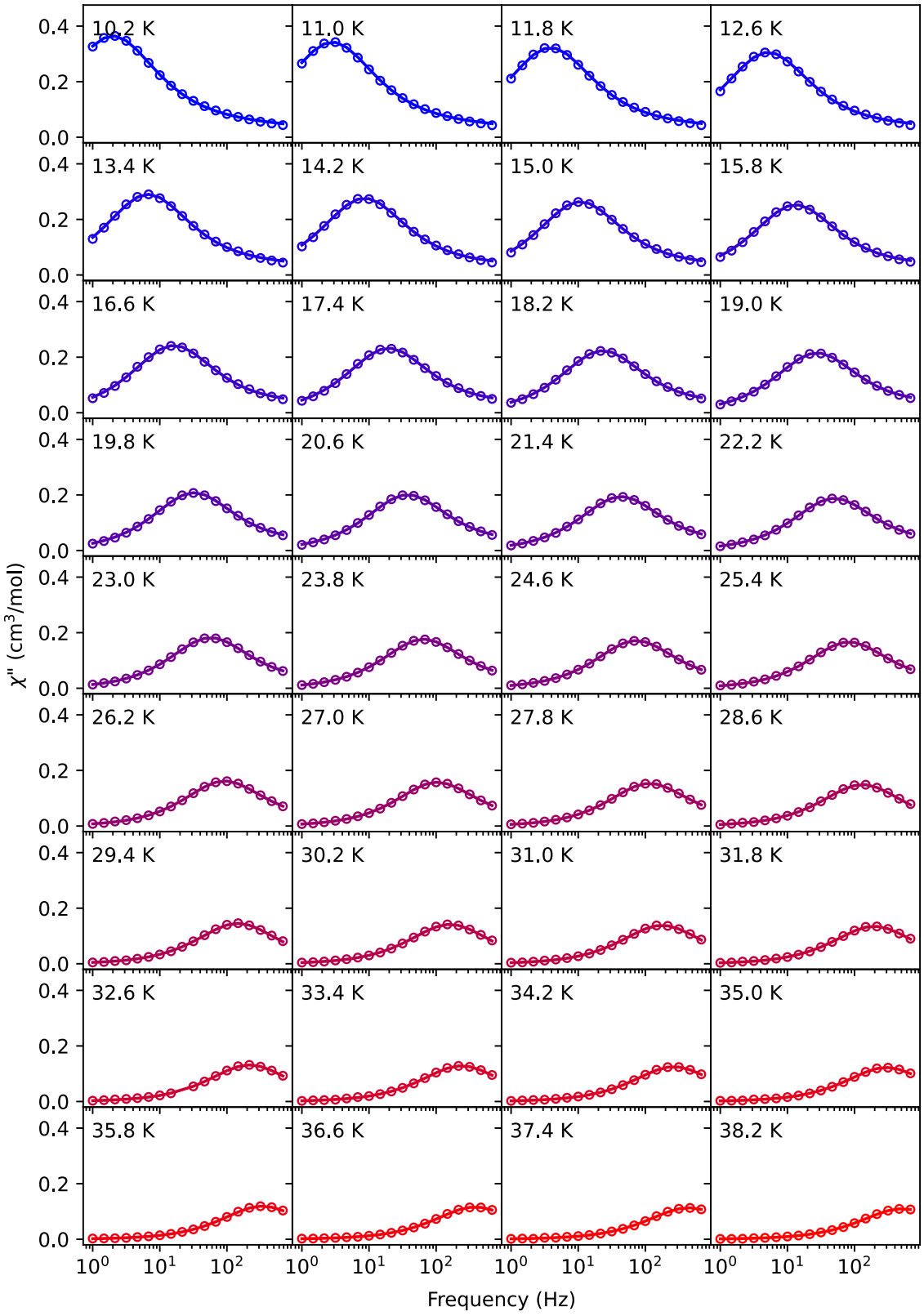

Figure S12. Frequency dependence of χ" for compound **1** measured at different temperatures ranging from 10.2 to 38.2 K under zero applied magnetic field. Solid circles represent experimental data, and lines correspond to theoretical fits using the Cole–Cole equation for multiple relaxation processes.

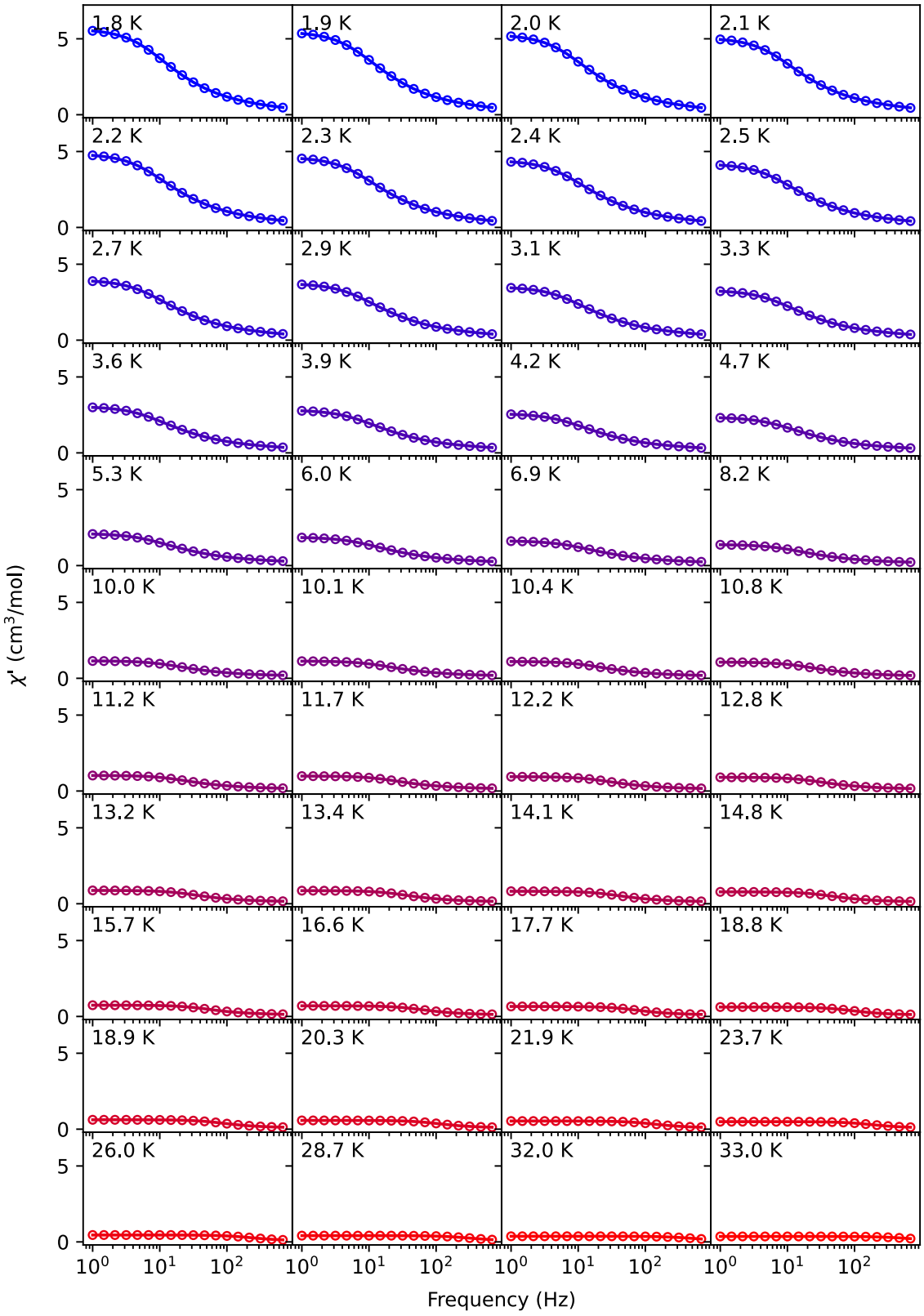

Figure S13. Frequency dependence of χ' for compound **2** measured at different temperatures ranging from 1.8 to 33 K under zero applied magnetic field. Solid circles represent experimental data, and lines correspond to theoretical fits using the Cole–Cole equation for multiple relaxation processes.

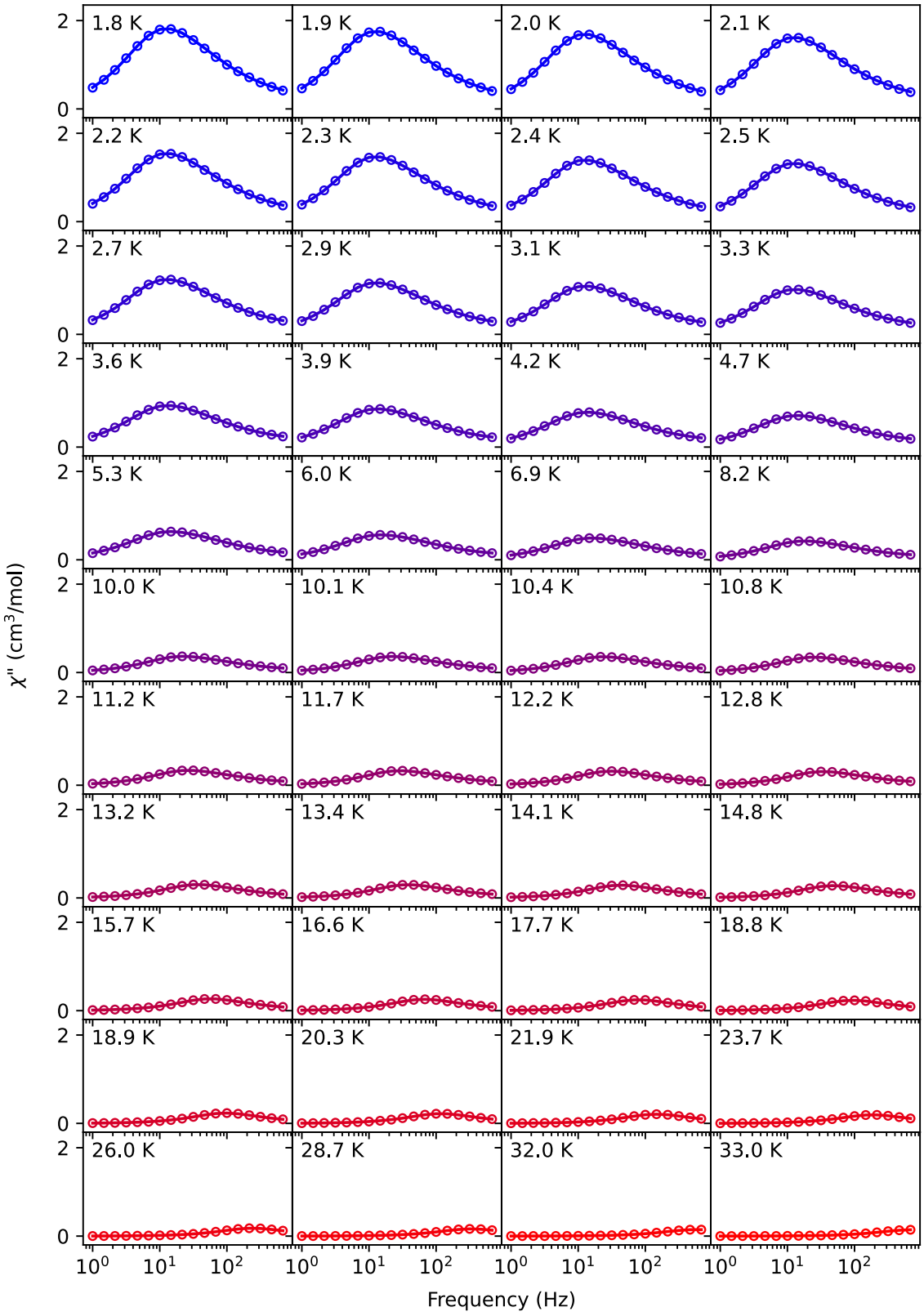

Figure S14. Frequency dependence of χ'' for compound **2** measured at different temperatures ranging from 1.8 to 33 K under zero applied magnetic field. Solid circles represent experimental data, and lines correspond to theoretical fits using the Cole–Cole equation for multiple relaxation processes.

Table S7. Crystal Field Parameters from XMS-CASPT2/RASSI-SO Calculations on **1, 2** and **2*.**

k	***q***	***B(k, q)***		
		1	**2**	**2***
2	0	-5.11	-5.05	-4.76
2	1	-8.72E-01	5.53E-01	4.32E-01
2	2	1.66	-3.00	-6.01E-01
4	0	-1.38E-02	-9.60E-03	-9.24E-03
4	1	1.38E-03	-1.69E-03	-3.29E-03
4	2	4.00E-03	5.79E-03	2.31E-04
4	3	-1.72E-03	-6.67E-05	-3.04E-03
4	4	-1.20E-02	-6.83E-03	1.05E-02
6	0	1.66E-07	1.29E-06	-2.00E-06
6	1	2.17E-05	-4.52E-06	2.10E-05
6	2	8.05E-06	1.66E-05	5.42E-07
6	3	-1.53E-05	-1.89E-05	-1.53E-05
6	4	-5.18E-05	-1.98E-05	3.29E-05
6	5	8.10E-06	4.62E-06	-2.54E-06
6	6	-1.26E-07	1.24E-05	1.15E-05

References

1 G. Li Manni, I. Fdez. Galván, A. Alavi, F. Aleotti, F. Aquilante, J. Autschbach, D. Avagliano, A. Baiardi, J. J. Bao, S. Battaglia, L. Birnoschi, A. Blanco-González, S. I. Bokarev, R. Broer, R. Cacciari, P. B. Calio, R. K. Carlson, R. Carvalho Couto, L. Cerdán, L. F. Chibotaru, N. F. Chilton, J. R. Church, I. Conti, S. Coriani, J. Cuéllar-Zuquin, R. E. Daoud, N. Dattani, P. Decleva, C. de Graaf, M. G. Delcey, L. De Vico, W. Dobrautz, S. S. Dong, R. Feng, N. Ferré, M. Filatov(Gulak), L. Gagliardi, M. Garavelli, L. González, Y. Guan, M. Guo, M. R. Hennefarth, M. R. Hermes, C. E. Hoyer, M. Huix-Rotllant, V. K. Jaiswal, A. Kaiser, D. S. Kaliakin, M. Khamesian, D. S. King, V. Kochetov, M. Krośnicki, A. A. Kumaar, E. D. Larsson, S. Lehtola, M.-B. Lepetit, H. Lischka, P. López Ríos, M. Lundberg, D. Ma, S. Mai, P. Marquetand, I. C. D. Merritt, F. Montorsi, M. Mörchen, A. Nenov, V. H. A. Nguyen, Y. Nishimoto, M. S. Oakley, M. Olivucci, M. Oppel, D. Padula, R. Pandharkar, Q. M. Phung, F. Plasser, G. Raggi, E. Rebolini, M. Reiher, I. Rivalta, D. Roca-Sanjuán, T. Romig, A. A. Safari, A. Sánchez-Mansilla, A. M. Sand, I. Schapiro, T. R. Scott, J. Segarra-Martí, F. Segatta, D.-C. Sergentu, P. Sharma, R. Shepard, Y. Shu, J. K. Staab, T. P. Straatsma, L. K. Sørensen, B. N. C. Tenorio, D. G. Truhlar, L. Ungur, M. Vacher, V. Veryazov, T. A. Voß, O. Weser, D. Wu, X. Yang, D. Yarkony, C. Zhou, J. P. Zobel and R. Lindh, *J. Chem. Theory Comput.*, 2023, **19**, 6933–6991.

2 L. F. Chibotaru and L. Ungur, *J. Chem. Phys.*, 2012, **137**, 064112.

3 L. Ungur and L. F. Chibotaru, *Chemistry – A European Journal*, 2017, **23**, 3708–3718.

4 P. Å. Malmqvist, B. O. Roos and B. Schimmelpfennig, *Chemical Physics Letters*, 2002, **357**, 230–240.

5 T. Shiozaki, W. Győrffy, P. Celani and H.-J. Werner, *J. Chem. Phys.*, 2011, **135**, 081106.

6 F. Neese, *WIREs Computational Molecular Science*, 2012, **2**, 73–78.

7 A. D. Becke, *Phys. Rev. A*, 1988, **38**, 3098–3100.

8 J. P. Perdew, *Phys. Rev. B*, 1986, **33**, 8822–8824.

9 C. van Wüllen, *J. Chem. Phys.*, 1998, **109**, 392–399.

10 S. Grimme, J. Antony, S. Ehrlich and H. Krieg, *J. Chem. Phys.*, 2010, **132**, 154104.

11 F. Weigend and R. Ahlrichs, *Phys. Chem. Chem. Phys.*, 2005, **7**, 3297–3305.
12 D. A. Pantazis and F. Neese, *J. Chem. Theory Comput.*, 2009, **5**, 2229–2238.
13 B. O. Roos, R. Lindh, P.-Å. Malmqvist, V. Veryazov, P.-O. Widmark and A. C. Borin, *J. Phys. Chem. A*, 2008, **112**, 11431–11435.